Report no. changed (Mar 2006): SM-349-UU

SACLANTCEN MEMORANDUM
serial no.: SM-349

SACLANT UNDERSEA RESEARCH CENTRE MEMORANDUM

DUSS97: SOURCE LOCALIZATION AND ENVIRONMENTAL INVERSION USING VERTICAL ARRAY DATA

A. Waldhorst, G. Haralabus

August 1998

Report no. changed (Mar 2006): SM-349-UU

SACLANT Undersea Research Centre
Viale San Bartolomeo 400
19138 San Bartolomeo (SP), Italy

tel: +39-0187-540.111
fax: +39-0187-524.600

e-mail: library@saclantc.nato.int

NORTH ATLANTIC TREATY ORGANIZATION

DUSS97: Source localization and environmental inversion using vertical array data

A. Waldhorst, G. Haralabus

The content of this document pertains to work performed under Project of the SACLANTCEN Programme of Work. The document has been approved for release by The Director, SACLANTCEN.

Jan L. Spoelstra
Director

intentionally blank page

DUSS97: Source localization and environmental inversion using vertical array data

A. Waldhorst, G. Haralabus

Executive Summary:

The primary task of passive and active sonars is the detection and localization of sound sources in an underwater environment. To fulfil this goal, different techniques can be used depending on the operational set up, the equipment, and the environmental conditions. Usually, when the acoustic field is received on a vertical line array, the preferred method is Matched Field Processing (MFP) which estimates the acoustic source location by comparing the actual field with synthetic data generated using a simulation model. In a shallow water environment, MFP has been shown to be effective in determining the target bearing, range, and depth. However, the performance of this method is strongly dependent on the accuracy of the calculation of the environmental parameters. Lack of knowledge of the channel propagation conditions often inhibits the utilization of MFP in shallow water. One way to overcome the environmental uncertainty problem is to use time efficient, global search methods to jointly estimate the source location and medium parameters. Global search algorithms in conjunction with MFP have been shown to significantly improve sonar system localization performance.

This report combines global search and MFP techniques to estimate source location and environmental parameters based on sea trial data collected by SACLANTCEN, in the Mediterranean in July 1997. The results are found to be in good agreement with ground truth values. A new analytical method for improving the performance of the classical MFP is introduced. Finally, instability problems due to the simulation geometry and the multi-frequency processing are discussed.

intentionally blank page

DUSS97: Source localization and environmental inversion using vertical array data

A. Waldhorst, G. Haralabus

Abstract:

Results on source localization and environmental inversion using experimental data acquired on a vertical line array are presented. Global inversion methods based on genetic algorithms are utilized to estimated the range and depth of a moving source located at approximately 9.0 km from the receiver array. Geometric and environmental parameters are estimated . The results are found to be in good agreement with observed values. However, the results are sensitive to minor changes in the simulation geometry and the number of significant frequencies processed. An advanced, non-parametric spectral estimation technique which improved the accuracy of the estimation of the covariance matrix did not enhance localization performance.

Keywords: Localization, global inversion, genetic algorithms, advance non parametric spectral estimation

Contents

1

Introduction

Matched Field Processing (MFP), a signal processing technique applied to acoustic fields measured on arrays of hydrophones, has been used primarily to solve the inverse source problem, i.e., to determine the unknown range, depth, and bearing of acoustic sources in a known propagation channel [1]. The basic principle of MFP is to cross-correlate the measured acoustic field with accurately modelled fields for which the parameters of interest are varied. MFP has enjoyed much success because it has demonstrated precise localization results in non-isotropic, non-planar acoustic fields. Also, MFP has been used as a tomographic method to solve the inverse environmental problem, i.e., to determine the characteristics of the unknown acoustic channel for known source location. However, it has been found that its performance is degraded significantly due to inaccuracies in the estimation of geometric or environmental parameters [2], [3].

To enhance localization performance by reducing the discrepancies between the assumed and the observed parameters, global inversion methods are introduced to jointly estimate the geometric and the environmental parameters. Often the global inversion problem is posed as a non-linear optimization problem. The parameters of interest assume discrete values within an interval according to *a priori* information. The MFP algorithm is repeated for different parameter sets. These sets are selected to optimize the objective function which provides a measure of similarity between the assumed and the observed parameter set. In most situations the model parameter space is factorially large and cannot be explored exhaustively. In a discrete space, where the notion of a continuing movement in a favourable direction does not exist, time efficient, global oprtimization algorithms, such as simulated annealing and genetic algorithms, are suitable.

In this paper, the MFP algothim is coupled to a genetic algorithm optimization method named SAGA (Seismo-Acoustic inversion using Genetic Algorithms) [4], [5] to process data sets acquired during the DUSS97 sea trial, south of the island of Elba, Italy, in the summer of 1997. The main objective is to localize a slowly moving source and at the same time provide an estimation of the environmental parameters for this area. The data were acquired for three positions of the target vessel which was towing the source. The acoustic field was received on a vertical array that spanned most of the water column. *A priori* knowledge of the geoacoustic parameters was limited and was primarily based on historical data.

The application of MFP combined with SAGA provided satisfactory localization and environmental results. The estimated positions of the acoustic source demostrated small deviations from baseline values. Environmental inversion was more challenging because of the complex structure of the subbottom layers which demonstrated sound speed values lower than those in the water column. Most of the parameters were close to the historical data with few examples of moderate deviation from baseline values. Localization and environmental inversion results appear to be sensitive to the number of frequencies. The best results were obtained by processing the best two frequencies. When the number of frequencies increased to six, the results were degraded. To increase the stability of the results, an advanced method to estimate the cross-spectral density matrices was employed. The new results were found to be similar to the previous ones. Also, the results were found to be sensitive to minor changes in the simulation geometry. Comparison between the forward field generated by SNAPRR [6] and that generated by C-SNAP [7] (this model is not incorporated into SAGA) suggests that variations of the parameter estimates may be related to imprecise estimation of the propagated sound field.

2

Experimental site and data collection

2.1 Description of the experiment

The sonar data sets were acquired on the last day of the summer cruise DUSS97 [8]. This sea trial was carried out between the 23 June and 3 July 1997 in an area south of the island of Elba.

Fig. 1 shows the experimental site bathymetry, the position of the vertical line array (VLA), the location where the sound velocity profile (SVP) was measured, the position from which core information was taken and finally the position of the target vessel. The SVPs were calculated using water temperature and pressure measurements (XBT) collected on the 3 July. The location of the measurements was the closest available to the propagation path between the source and the receiver, i.e. 42°: 30.373′ N, 10°: 20.881′ E at 10:12:04. The depth at this position was approximately 203 m. The target vessel followed a course from 42°: 29.4690′ N, 10°: 18.9390′ E, corresponding to 11:10:00 to 42°: 29.6240′ N, 10°: 19.2860′ E at 11:14:00. The location of the vertical array was 42°: 33.962′ N, 10°: 21.959′ E. The depth at this position was 161 m.

All coordinates were derived from the GPS during the cruise. The starting and final points of the tracks corresponded to approximate distances 9.3 km and 8.8 km respectively from the vertical line array. These source-receiver distances were also in good agreement with the values derived from the travel time of the ping from the target to the array. In the latter calculation, a (constant) sound speed in water of 1510 m/s was assumed. Since this value was measured for the correct source and receiver depth (see Fig. 3), it corresponds to the phase velocity of the direct path wave. The water depth along the source track was assumed to be approximately 200 m, as indicated by charts. The source depth was determined by underwater pressure measurements and sampled every 5 s during the experiment. It varied from 100 m to 102.5 m (within certain error bounds due to the limited accuracy of the measurement process).

Fig. 2 shows the source depth as a function of time in the relevant recording interval specified above. Zero s on the time axis corresponds to 11:09:00. Table 1 summarizes the measured source positions at the times corresponding to the 3 data sets investigated in this study. Fig. 1 also indicates that the signal propagation path from

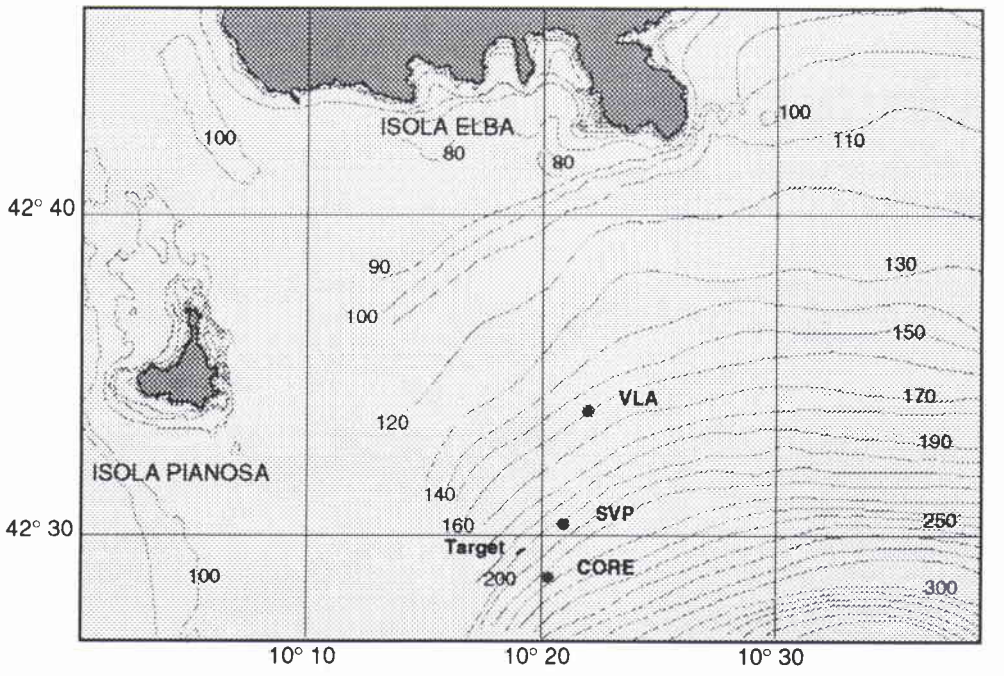

Figure 1 *Bathymetry, equipment locations and target vessel track.*

the source to the array passes an almost linearly upsloping bottom with increasing distance from the transmitter. The bathymetry variation along this track is about 40 m over 9 km in range.

DATA SET	SOURCE RANGE	SOURCE DEPTH
1	9289 m	102.3 m
2	9055 m	102.0 m
3	8820 m	101.88 m

Table 1 *Positions of the source for the 3 data sets examined.*

The sound velocity profile is plotted in Fig. 3. It can be seen that the channel property is characterized by a downward refracting sound propagation condition typical of the mediterranean summer. It shows nearly isovelocity down to 23 m, a strong thermocline to about 55 m, which finally approaches a second almost isovelocity interval extending to about 190 m. Hence, a certain degree of bottom interaction is expected. However, with the source location approximately in the middle of the water column, the acoustic energy propagates mainly at the mid depths. During DUSS97, no core measurements were taken. However, general environmental information is known from previous experiments. The bottom is covered with low sound velocity clay and sandclay layers overlying a higher speed silt layer ([9], [10], [11], [12]). Information on geophysical properties of the sediment was taken from a core

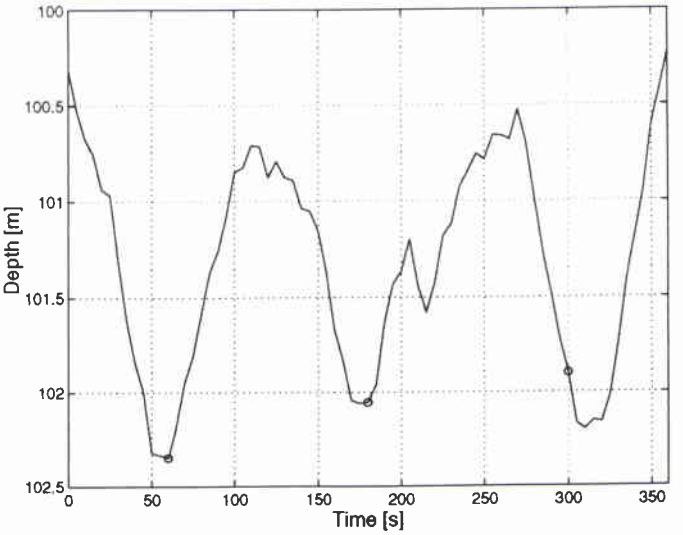

Figure 2 *Depth variation of the sound source versus time. The circles indicate the source depth during the first pings for the three cases investigated here.*

collected on 20 February 1995, at 42°: 28.716′ N, 10°: 20.214′ E which provides sediment sound speed information for 1.9 m beneath the water sediment interface (Fig. 4).

2.2 Source characteristics

A sound source towed by a support ship along the course described served as the target. A nonstationary broadband pulse of one second duration was transmitted. It was repeated at 15 s intervals starting at 11:10:00. The ping was produced using a linear frequency modulated waveform of 150 Hz bandwidth and 950 Hz centre frequency. The estimated spectrum of the transmitted ping is shown in Fig. 5.

2.3 Receiver characteristics

The total aperture of the array was 15.5 m with 32 hydrophones at 0.5 m spacing between sensors. The bottom hydrophone (referred to as the first sensor) was located at 108.75 m depth; consequently the top sensor (corresponding to sensor 32) was placed at the depth of 93.75 m yielding 101m depth for the acoustic centre of the array. These are approximate values because the actual depths may deviate from those presented primarily due to current induced array tilt and measurement inaccuracies.

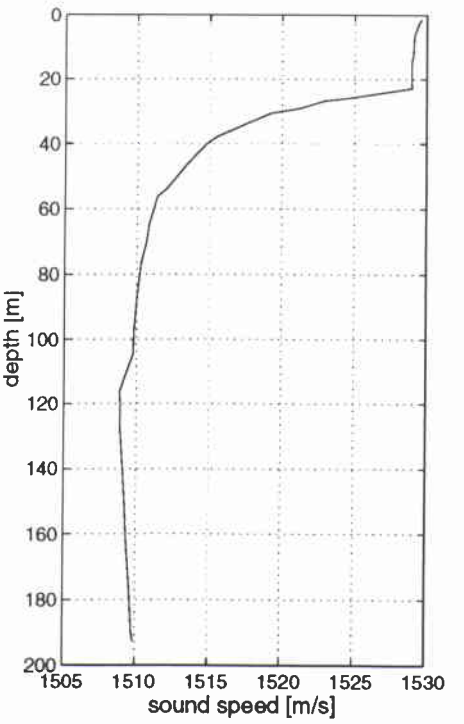

Figure 3 *Sound velocity profile in the water column that was used at the baseline model.*

2.4 Preprocessing of the array data

The received signal was sampled at the vertical array at 12 kHz and passed through a linear phase, digital 255 coefficient, FIR bandpass filter with the following specifications: centre frequency 950 Hz and the 3 dB bandwidth 240 Hz. In the passband a ripple of 0.1 dB was tolerated. The stopband attenuation was 60 dB and the total transition bandwidth was 120 Hz. For data storage economy, data sequences were undersampled by a factor of ten, yielding 1200 Hz for the new sampling frequency. The relevant part of the received signal spectrum is confined between 875 Hz and 1025 Hz (Doppler shift and other nonlinear effects are neglected). Due to undersampling, this original bandlimited signal spectrum is mapped to the interval between 175 Hz and 325 Hz as an inverted and conjugate complex version of the original one. To compare the received with the modelled data the signal was restored to the original frequency band.

Fig. 6 shows a spectral estimation of a single ping received by the 16th array hydrophone. By comparison with the spectrum of the transmitted ping in Fig. 5, two main features can be observed. First, the spectral cancellation at certain frequencies due to multipath effects. Second, there is an increasing attenuation of signal com-

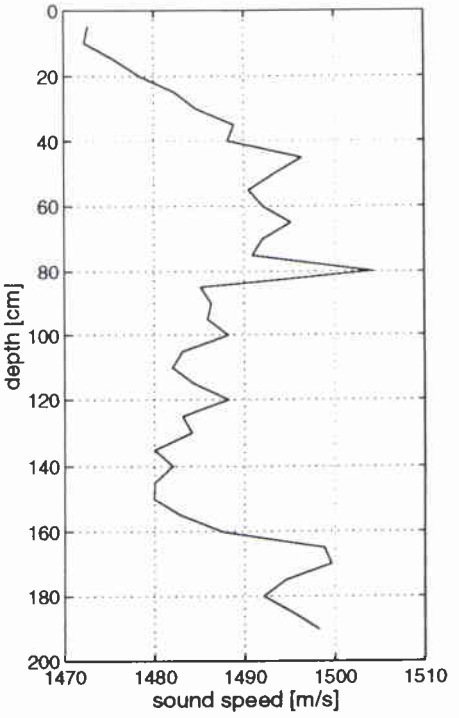

Figure 4 *Sound velocity profile in the sediment layer.*

ponents belonging to higher frequencies. The latter observation is due to increased bottom penetration of the higher modes.

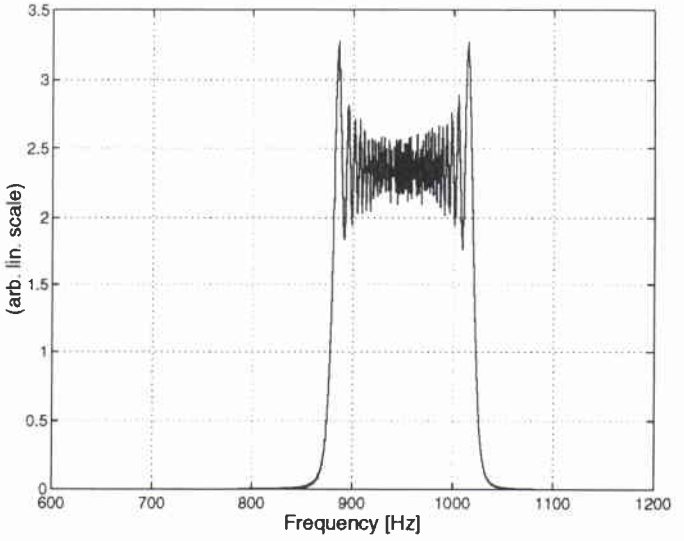

Figure 5 *Estimated spectrum of the transmitted ping using a rectangular window.*

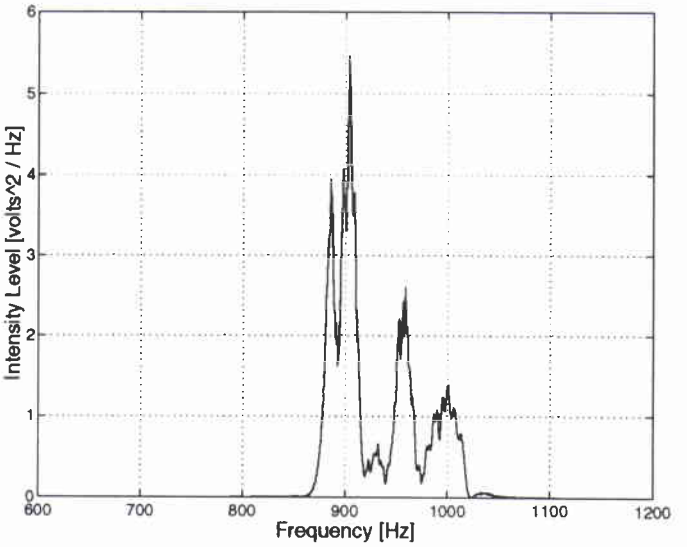

Figure 6 *Estimated spectrum of a received ping recorded in the first data set using a rectangular window.*

3 Source localization and environmental inversion

In this section we outline the steps taken to address the source localization and the environmental inversion problem. Generally, the idea is to incorporate as much *a priori* information about the channel as possible so that the localization method can exploit this knowledge in order to achieve reliable localization results.

3.1 Matched field processing

The conventional way to process acoustic signals received at a vertical array is the MFP technique. In this scheme, a mathematical channel model is incorporated into the process, which uses the channel parameters as an input, to predict the pressure field observed at the receiver. The actual source location is the one which yields the best match between actual and modelled data.

However, the process has to deal with environmental uncertainty. In previous studies inaccurate assumptions of the channel parameters severely degraded system performance. This characteristic of matched field processing is termed the *mismatch* problem [13], [14]. One way to overcome this difficulty is to design a processor which is robust against mismatch and capable of target localization and acoustic channel parameter estimation (or environmental *inversion*) in parallel. In this technique, the channel is discretized in the following way. First, fixed search intervals for the channel parameters are defined. Second, each parameter can only assume a certain number of *discrete* values within its interval. The *a priori* information is in this case only used to set up interval bounds for parameter optimization.

3.2 Global optimization using SAGA

To deal with the problem of searching the multi-dimensional space for the correct parameter set, smart optimization schemes were introduced, one of which is based on genetic algorithms (GA). In this study, the genetic algorithm implemented in the SAGA (*Seismo-Acoustic inversion using Genetic Algorithms*) package, which incorporates several different types of forward models [4], [5] is used.

3.2.1 Signal processing in the frequency domain

In matched field processing, real and modelled data are compared in the frequency domain in the following manner: The sampled array data is denoted by $\underline{x}(t) = (x_1(t), .., x_N(t))'$ with $t = 0, .., T-1$, where N is the number of sensors and $T \in \mathbb{N}$ the total number of data samples. We assume that the received sequences contain a superposition of a deterministic transient part (a linear filtered version of the ping) and a — at least within the analysis window — stationary noise component. The received noise consists mainly of sensor and ambient noise.

As a first step, each sensor signal is multiplied by a smooth window $w(t)$ where $w(t) = 0$ for $t \notin [0, 1]$ and afterwards Fourier transformed using

$$\underline{X}_T(\omega) = \sum_{t=0}^{T-1} w\left(\frac{t}{T}\right) \underline{x}(t) \mathrm{e}^{-j\omega t}. \tag{1}$$

In the experiments, a hamming window was used for $\underline{w}(t)$. Based on Eq. (1), an estimate of the *cross spectral density matrix* (sometimes also referred to as the *spatial covariance matrix*) can be obtained from the periodograms:

$$\mathbf{I}_{\underline{X}_T}(\omega) = \underline{X}_T(\omega) \underline{X}_T{}^*(\omega), \tag{2}$$

so that

$$\hat{\mathbf{C}}_{\underline{X}}(\omega) = \mathbf{I}_{\underline{X}_T}(\omega). \tag{3}$$

In Eqs. (2) and (3) the asterisk denotes the conjugate transpose operation and $\hat{\mathbf{C}}_{\underline{X}}(\omega)$ signifies the estimate of $\mathbf{C}_{\underline{X}}(\omega)$ which is the true spectral density matrix.

For the environmental modelling aspect of the problem it is assumed that the channel is described by the model vector $\underline{\vartheta} = (\vartheta_1, ..., \vartheta_M)'$. The objective function Φ to be optimized depends on the predicted field vectors $\underline{p}(\underline{\vartheta}, \omega)$ and the estimated spectral density matrices $\hat{\mathbf{C}}_{\underline{X}}(\omega_i)$ calculated from the received data. Here, $\omega_i, i = 1, ..., P$ denotes selected frequency bins. For the present analysis the two *most significant* (highest power) frequencies have been determined and used in the localization process. At these frequencies, the array averaged spectral power of the sensor signals was maximized.

The problem is to find the model vector $\underline{\vartheta}$ that minimizes the objective function Φ.

3.2.2 The Bartlett-processor

In our study, the following broadband version of the Bartlett-power (see also, e.g. [15]) was used for the objective function:

$$\Phi(\underline{\vartheta}) = \sum_{i=1}^{P} \left[\mathrm{tr}\, \hat{\mathbf{C}}_{\underline{X}}(\omega_i) - \frac{\underline{p}^*(\underline{\vartheta}, \omega_i) \hat{\mathbf{C}}_{\underline{X}}(\omega_i) \underline{p}(\underline{\vartheta}, \omega_i)}{\underline{p}^* \underline{p}} \right] \tag{4}$$

where *tr* indicates the trace of the covariance matrix. It can be shown, that this processor is related to the broadband log-likelihood function, ([16], Eqs. (25),(26)) under certain assumptions concerning signal and noise characteristics.

3.2.3 The Genetic Algorithm and its parameter settings

The global optimization procedure using genetic algorithms (GA) [17] and [5]) can be characterized as a stochastic, directional search applying principles of biological evolution. The parameter search space over which the optimization problem is formulated is *discretized.* This is due to a binary coding of the parameter values using a predefined number of bits. For instance, throughout all the experiments made in this study, 7 bits were used to code the parameter values yielding 128 states per parameter. Then, from all possible model vectors (or unknown parameter vectors), an initial set, called a *population*, is selected. Each of the q model vectors in this population is refered to as a *member.* Using the objective function Φ, a *fit* of each member is computed, based on the distance between the observed and the computed data. During several *evolutionary* steps the original population evolves to become more fit. Each of these steps involves the selection of a number of members according to their fitness, which become the *parent* model vectors for the next step (or *generation*). These parents are then combined pairwise to form a set of *children.* This combination is performed according to certain, biologically motivated principles. Operators of this kind are *crossover* and *mutation.* The effects of these operators are controled by the crossover and mutation *rate.* A part of the population is replaced by the children to increase the match between synthetic and observed data. The size of this part is determined by the *reproduction size* and provides that the fittest individuals 'survive' in the course of the evolutionary steps.

In all the localization experiments described below, the following parameters have been used for the Genetic Algorithm: The population size was 64, crossover rate 0.8, mutation probability 0.05 and reproduction size 0.5. The number of parallel populations was set at 12. With the selected number of 3000 iterations which is equivalent to the number of forward modelling calls per population, a total of 36000 forward model runs is carried out per frequency.

3.2.4 Choice of the forward model

In general, the underwater acoustic shallow water waveguide is characterized by fading, time-dispersive, frequency-dependent and boundary condition sensitive time-varying characteristics. A detailed modelling of all relevant features is impossible as only relatively coarse knowledge is available. For instance, the assumption has to be made that the spatial samples of the geoacoustic properties are representative.

An appropriate modelling of not only the bottom topography but also of the *range dependent* bathymetry and geoacoustic properties is essential for matching pressure measurements for all frequencies and sensor locations [11], [14]. It is therefore evident that an appropriate range dependent forward model has to be selected in order to generate the synthetic data to predict the measurements at the array site. The SACLANTCEN normal mode acoustic propagation model SNAP [6] is used since it is the only suitable range dependent forward model built into SAGA (where it is referred to as SNAPRD). SNAP is based on mode theory and the environment is represented by three layers: the water layer with pressure release boundary conditions at the surface, a fluid sediment layer and a homogeneous solid halfspace. In each layer, the density and the volume attenuation are assumed to be constant. In the first two layers, the sound velocity may vary arbitrarily with depth. Parameters may also vary with range. These range dependent characteristics are treated by dividing the range into a number of segments containing different, but within each segment, range independent parameters. In each segment, the algorithm solves for the modes separately. The individual solutions are afterwards combined using the *adiabatic approximation*, which does not take into account the energy transfer between modes of different order, when coupling the solutions in the segments, to obtain the total field (see, e.g. [18]). Moreover, in this model only the modes corresponding to the discrete (horizontal) eigenvalue spectrum are taken into account, leading to inaccurate results in the nearfield of the source. Loss mechanisms are treated approximately in a perturbative manner.

In order to parametrize the channel within the scope of the forward model SNAPRD, the following steps have been taken. To model the upsloping bottom, the region was devided into 2 range independent segments in which the same sound velocity profile (Fig. 3) was used since no more detailed information was available. The profile was simply truncated or extrapolated (using the same value) for the required depth of the particular segment. The depth in the first segment which is the segment containing the source at range zero, remained constant in the processing of the 3 files. The depth of the second segment was changed for the different data sets to obtain acceptable results. The ranges of the two segments were always identical but also changed per data set. Table 2 summarizes the segment lengths and depths applied in propagation forward modelling for the 3 data sets. The depth of the second segment was selected to correspond to the depth required by the slope at the

given range from the target vessel (Fig. 1).

	DATA SET 1	DATA SET 2	DATA SET 3
Range, segm. 1& 2	10 *km*	7.5 *km*	9 *km*
Depth, segm. 1	200 *m*	200 *m*	200 *m*
Depth, segm. 2	156 *m*	170 *m*	160 *m*

Table 2 *Segment geometries used in the 3 baseline models.*

3.2.5 *Error analysis using* a posteriori *statistics*

In order to analyze the accuracy, uniqueness and uncertainty of the estimates obtained, *a posteriori* probabilities of the parameters are estimated. The model vectors are sampled during the evolution process and weighted according to their fitness and to the Boltzmann distribution. These scaled model vectors serve as an estimate of the sampled multivariate *a posteriori* probability density function, from which the marginal density functions which are used in the analysis can be calculated ([5]).

According to estimated marginal *a posteriori* distributions the variances of the parameters can be assessed. These variances may be caused by 3 factors [14]: noise and modelling induced variance.

3.3 *Experimental results*

In this section, we present the localization results obtained for the 3 data sets corresponding to the source positions in Table 1. We also show the most important channel and the bottom parameters that resulted from the parallel inversion procedure. In all experiments the spectral density matrices computed for the two most significant frequencies were used. The results are shown in terms of estimated /empha posteriori distributions as discussed above.

3.3.1 *Localization*

In all the localization experiments we searched within a 1 km interval in range from 8.5 km to 9.5 km. The search interval for the source depth was defined to range from 90 m to 110 m.

The estimated source location derived from the first data set is shown in Fig. 7. The vertical lines indicate the initial search values (baseline model). By comparison

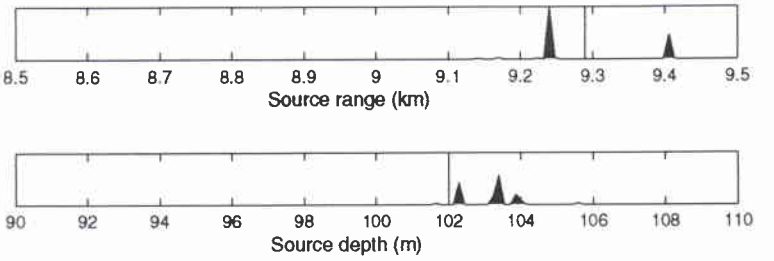

Figure 7 *Estimated target position for first data set.*

with the measured values presented in table 1, good agreement can be observed. The corresponding results for the other two data sets are shown in Fig. 8 and Fig. 9. Their deviation from the measured positions is somewhat larger, especially for the intermediate localization, but they still lie within acceptable error bounds (about 100 m difference in range and 2.5 m in depth).

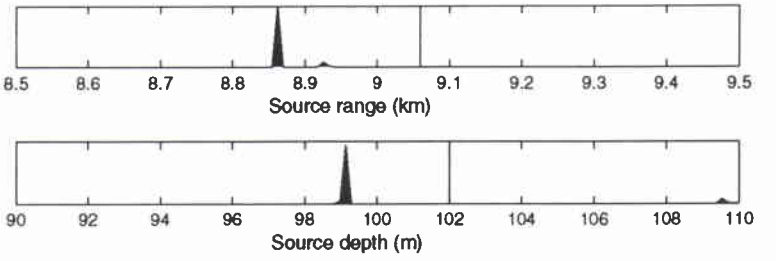

Figure 8 *Estimated target position for second data set.*

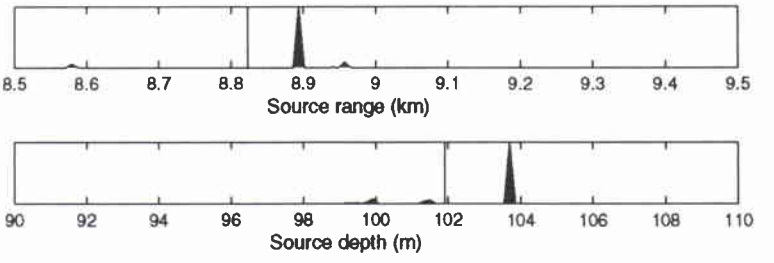

Figure 9 *Estimated target position for third data set.*

3.3.2 Environmental inversion

The results of the environmental inversion that correspond to the target position estimates presented above are shown in the Figs 10, 11 and 12. The starting values for the GA inversion representing the baseline model (vertical lines in the graphs)

were taken from the historical data presented in the first section (see Fig. 4 and [9]). In the baseline model applied to the first file, the sediment was represented by 4 layers with 4 different sound speeds. More details concerning this part of the baseline model are shown in Table 3. For the inversion of the remaining two data sets, a two layer sediment was used with the specifications given in Table 4. The search bounds for all parameters are identical to the bounds of the displayed intervals.

MODEL PARAMETER	VALUE
Sediment	
Sound speed c_0	1465 m/s
Sound speed c_6	1505 m/s
Sound speed $c_{7.5}$	1488 m/s
Sound speed c_{15}	1500 m/s
Density	1.5 g/cm^3
Attenuation	0.06 dB/λ
Thickness	15 m
Bottom	
Sound speed	1520 m/s
Density	1.8 g/cm^3
Attenuation	0.1 dB/λ

Table 3 *Sediment and bottom parameters for the first baseline model. Sound speeds refer to compressional waves. Subscripts denote the sediment depth.*

MODEL PARAMETER	VALUE
Sediment	
Sound speed c_0	1470 m/s
Sound speed c_{10}	1500 m/s
Density	1.5 g/cm^3
Attenuation	0.06 dB/λ
Thickness	10 m
Bottom	
Sound speed	1537 m/s
Density	1.8 g/cm^3
Attenuation	0.1 dB/λ

Table 4 *Sediment and bottom model with two sediment layers.*

In all 3 cases the *a posteriori* distributions have a distinct peak which indicates the estimated parameter value.

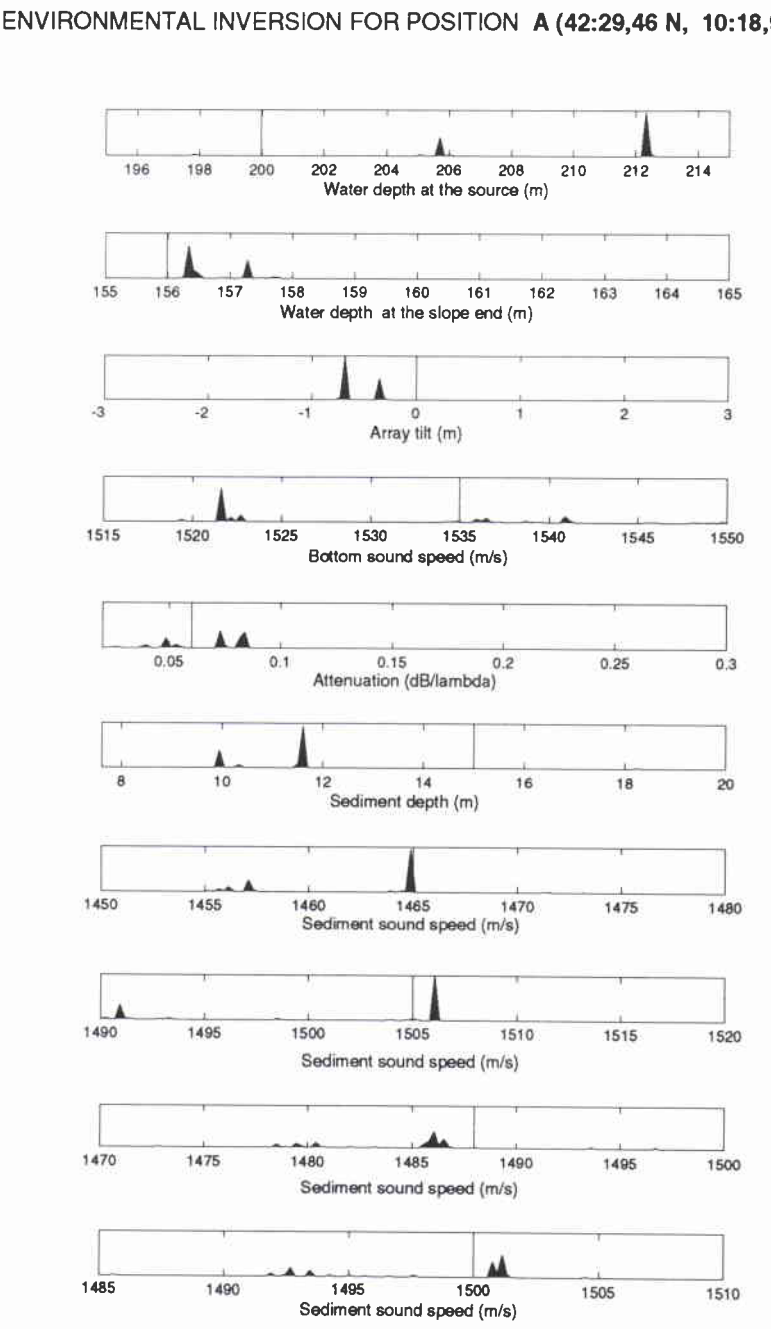

Figure 10 *Results of environmental inversion for first data set.*

ENVIRONMENTAL INVERSION FOR POSITION **B (42:29,54 N, 10:19,11 E)**

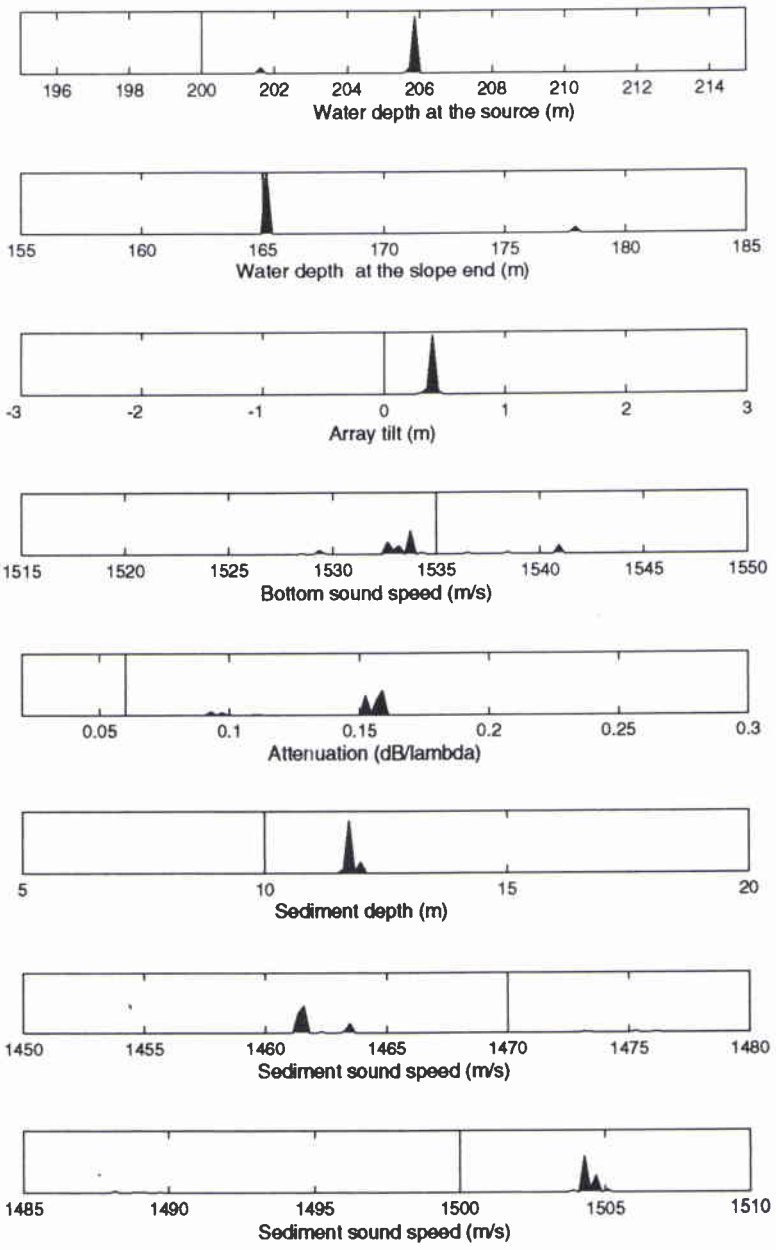

Figure 11 *Results of environmental inversion for second data set.*

ENVIRONMENTAL INVERSION FOR POSITION **C (42:29,62 N, 10:19,28 E)**

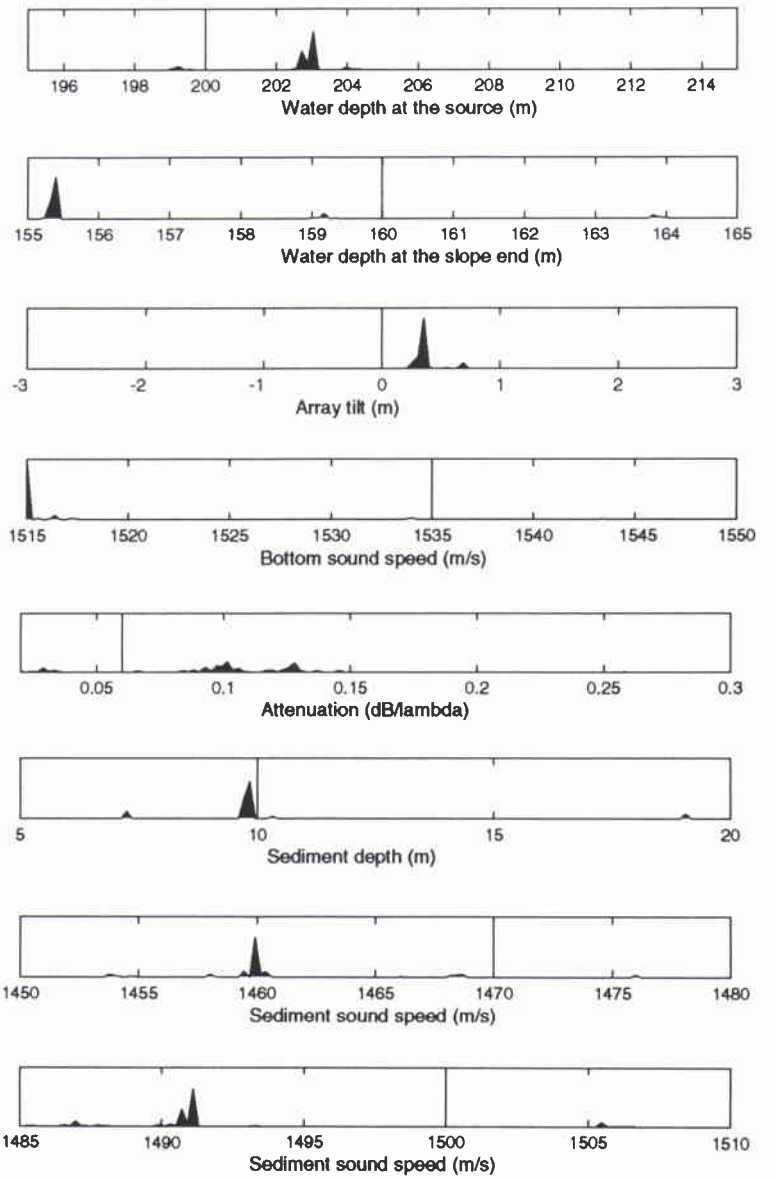

Figure 12 *Results of environmental inversion for third data set.*

4

Frequency and simulation instabilities

Although the results presented in the last section show good agreement with both the source position and the environmental parameters, they demonstrate unsual instability related to the number of frequencies processed and to changes in the simulation geometry.

To study the frequency effect we increase the number of frequencies from two to six. It is expected that the variance of the estimated parameters decreases with increasing frequency number. [19]. Provided that the forward modelling scheme is sufficiently accurate, a broadband approach should lead to more stable localization results.

Fig. 13 (top) shows the comparison of localization results for the second source position using two and six-frequencies. In the six frequency case, the deviation of the estimated parameters from the baseline values increases. In this case there are two dominant peaks, neither of which corresponds to the actual source distance. Also an unexpected deviation from the previously presented localization estimates was observed when the sector length (and the corresponding depth in the second segment) was slightly changed. This effect is illustrated in Fig. 13 (lower). A sector length of 7 km instead of 7.5 km was used. The range estimate of the target position is correct, whereas the depth estimate differs by more than 10 m.

The fact that the higher amount of frequencies could not stabilize the estimates and that a slight change in sector length causes an increased bias suggest that the chosen forward model SNAPRD might not be well suited to the given environment. To evaluate the accuracy with which the forward field is calculated, propagation loss measures obtained using SNAPRD are compared to those generated using C-SNAP. C-SNAP is a normal mode propagation model which allows mode coupling (energy transfer between modes) and significant range segmentation to deal with range dependent bathymetries. C-SNAP is considered one of the most accurate full field models for the calculation of the forward field in a range dependent environment. It must be noted that the utilization of C-SNAP by SAGA has not yet been implemented. Fig. 14 shows propagation loss versus range plots produced by SNAPRD (solid) and C-SNAP (dotted line). The operating frequency is 950 Hz (most significant frequency), the source depth is 102 m, and the range 10 km. Beyond 6 km, the calculations differ significantly. Plots of depth versus propagation loss at 9.3

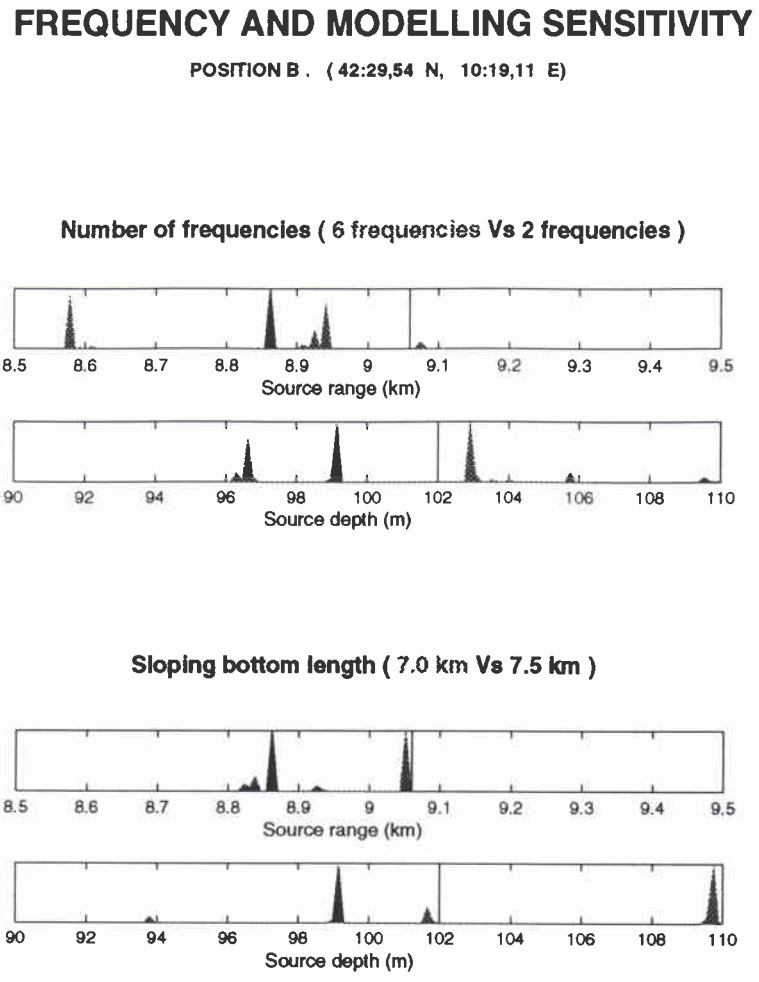

Figure 13 *Variance and bias effects caused by a higher number of frequencies and by changing the length of the sloping bottom in the model.*

km are shown in Fig. 15. The frequency remains 950 Hz. The discrepancies in the calculations of the two models are evident in the entire water column.

There are no alternatives in the choice of propagation model because at present, SNAPRD is the only range dependent model implemented in SAGA. Thus the only way to improve upon the results obtained, is to control variability due to frequency and reduce "noise" in the algorithm in the form of spectral estimation errors. An advanced algorithm has therefore been developed for the estimation of cross-spectral density matrices.

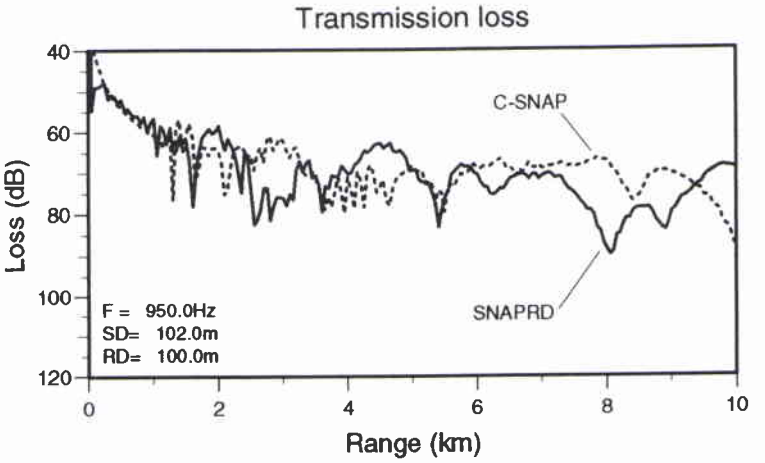

Figure 14 *Transmission loss versus range comparison using SNAPRD and C-SNAP models.*

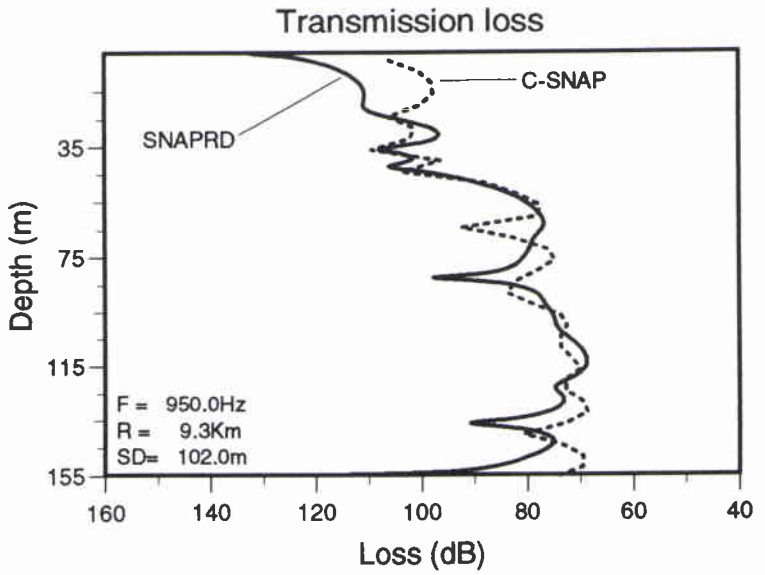

Figure 15 *Transmission loss versus depth comparison using SNAPRD and C-SNAP models.*

5

Advanced nonparametric spectral estimators

In this section we briefly discuss a more sophisticated method to estimate cross spectral density matrices of the observed sensor data and compare the obtained localization results to the estimates of the last section.

5.1 Fourier transformation of the array data

Analogous to the former method, the data are windowed prior to Fourier transformation. The difference is that instead of one window, several windows $w_l(t)$ ($l = 1, ..., L$), where $w_l(t) = 0$ for $t \notin [0, 1]$ can be used:

$$\underline{X}_T^l(\omega) = \sum_{t=0}^{T-1} w_l\left(\frac{t}{T}\right) \underline{x}(t) \mathrm{e}^{-j\omega t},\ l = 1, ..., L. \tag{5}$$

Based on Eq.(5) the matrix of periodograms

$$\mathbf{I}_{\underline{X}_T}^l(\omega) = \underline{X}_T^l(\omega) \underline{X}_T^{l\,*}(\omega) \tag{6}$$

can be computed and serves as a basis for the spectral estimator. The periodogram matrix does not yield good estimates for the spectral density matrix as the observation time T and the choice of the window has no effect on its quality (i.e. its variance) [20].

5.2 Spectral estimation using orthonormal windows

The method that was applied here is the *multiple window technique* proposed by [21]. Unlike the estimator used previously, this procedure allows bias control (i.e. the systematic error) and variance properties. In this scheme, the *discrete prolate spheroidal sequences*, DPSS [22] serve as the data tapers before computing the Fourier transform. The spectral estimator uses a weighted averaging of periodograms to asymptotically maximize the signal power in a predefined frequency band for a specified time-bandwidth product [23]. The following steps are performed:

1. A normalized analysis bandwidth $2W$ with $0 < W < 0.5$ is selected. If $T \in \mathbb{N}$ denotes the number of samples selected for the estimation. Typical bandwidths lie between $\frac{2}{T}$ and $\frac{4}{T}$. The maximum number L of tapers to be used is bounded above by the time-bandwidth product $2TW$. A smaller value of W results in higher resolution of spectral estimates but also increases variance. With the chosen values for W and T the DPSS tapers $w_l(T, W; t)$ are computed for all orders $l = 1, ..., L < 2TW$.

2. We compute the *eigenspectra* $\hat{\mathbf{C}}^l_{\underline{X}}(\omega)$

$$\hat{\mathbf{C}}^l_{\underline{X}}(\omega) = \mathbf{I}^l_{\underline{X}_T}(\omega) \tag{7}$$

   where Eq.(5) with the DPSS tapers $w_l\left(\frac{t}{T}\right) = w_l(T, W; t)$ and Eq.(6) are now used to compute the periodogram matrices. Strictly, a factor $e^{-j\omega t}/\sqrt{T}$ is omitted when using Eq. (5) as it is of no importance for spectral analysis applications.

3. The average over the estimated eigenspectra is computed:

$$\hat{\mathbf{C}}_{\underline{X}}(\omega) = \frac{1}{L} \sum_{l=1}^{L} \hat{\mathbf{C}}^l_{\underline{X}}(\omega) \tag{8}$$

The main advantages of this technique are as follows. For a fixed value of W the variance of the estimator decreases with $1/T$. The spectral resolution is well defined to be $2W$ and can be controlled by the user. It can also be shown that the estimator's bias is controled by the choice of the parameters. The estimator is asymptotically consistent. All samples in the analysis window are equally weighted in the process (Fig. 16). Samples close to the interval bounds are not penalized in this technique ([21], [23]).

5.2.1 Computation of the DPSS

SLEPIAN [22] defines the data tapers $\underline{w}_l(T, W) = (w_l(T, W; 0), ..., w_l(T, W, T-1))'$, as the solutions to the following symmetric Eigenvalue problem:

$$\mathbf{T}\underline{w}_l(T, W) = \lambda_l(T, W)\underline{w}_l(T, W) \tag{9}$$

Only the most dominant eigenvalues ($l = 1, ..., L \leq 2TW$) are taken into account (see above). The matrix $\mathbf{T}$ is a symmetric, positive definite Toeplitz matrix and its elements are given by

$$T_{ij} = \begin{cases} \frac{\sin 2\pi W(i-j)}{\pi(i-j)}, & (i \neq j) \\ 2W, & (i = j) \end{cases} \qquad (i, j = 1, ..., T) \tag{10}$$

The Slepian sequences are orthonormal functions. When the taper order l is an odd number, the function is even, and vice versa. To avoid numerical problems in calculating the eigenvectors directly using the *power method* which are caused by the fact that the most dominant eigenvalues are close to one, we apply a (modified) *inverse iteration* implementation to a matrix $\mathbf{M}$ given by $\mathbf{M} = \mathbf{T} - \mathbf{I}$ (in the following, the arguments T and W are omitted):

$$\mathbf{M}\underline{w}_l^{k+1} = \lambda_l \underline{w}_l^k, \qquad (k = 1, 2, ...; l = const.) \tag{11}$$

to solve for the l-th eigenvector iterating over k. This procedure is equivalent to the power method applied to $\mathbf{M}^{-1}$ [24]. Now the eigenvalues $1/(1 - \lambda_l)$ of $\mathbf{M}^{-1}$ have considerably different magnitudes than those in the original problem. The recursion (11) can effectively be solved for $\underline{w}_l^{k+1}$ using LEVINSON'S algorithm for the general right hand side problem. Every time a new taper is to be computed, a new starting vector $\underline{w}_l^1$ is produced by initializing it with an even or odd function (depending on the parity of l). After each iteration, (11) the new candidate eigenvector $\underline{w}_l^{k+1}$ is orthonormalized together with the space spanned by the previously computed eigenvectors.The eigenvector is scaled and *polarized* according to SLEPIAN'S convention [25]. The terminating criterion is satisfied when the norm of the residual $\|\underline{w}_l^{k+1} - \underline{w}_l^k\|_2$ reaches a predefined lower bound.

Fig. 16 shows a plot of the $L = 4$ DPSS data tapers ($l = 1, ..., L$) resulting from $T = 1024 \approx 0.8533s$ and $2W = \frac{5}{T} \approx 5.86$Hz.

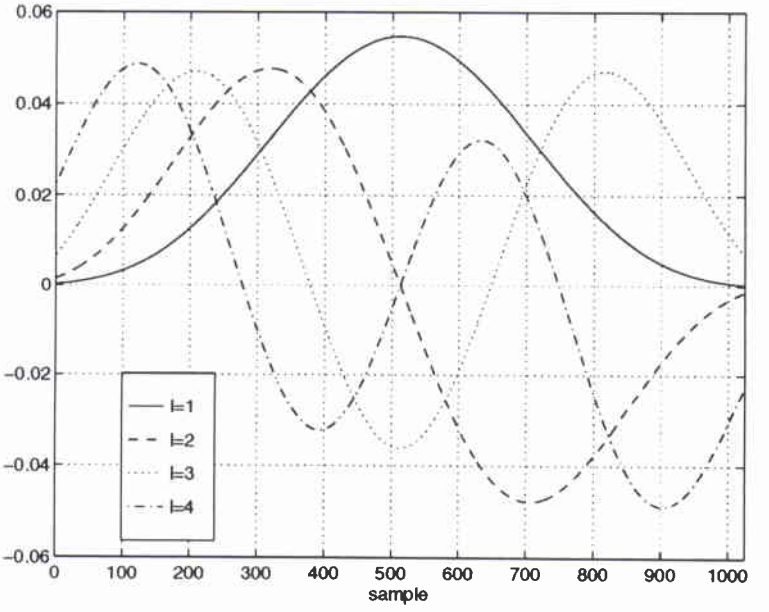

Figure 16 *DPSS data tapers with parameters* $T = 1024$, $2W \approx 4.88 \cdot 10^{-3}$, $L = 4$.

5.3 Experimental results

The localization estimates achieved with the described technique are presented in Fig. 17. The results for the 3 target positions show that no improvement could be obtained using the multi-taper (four tapers) technique.

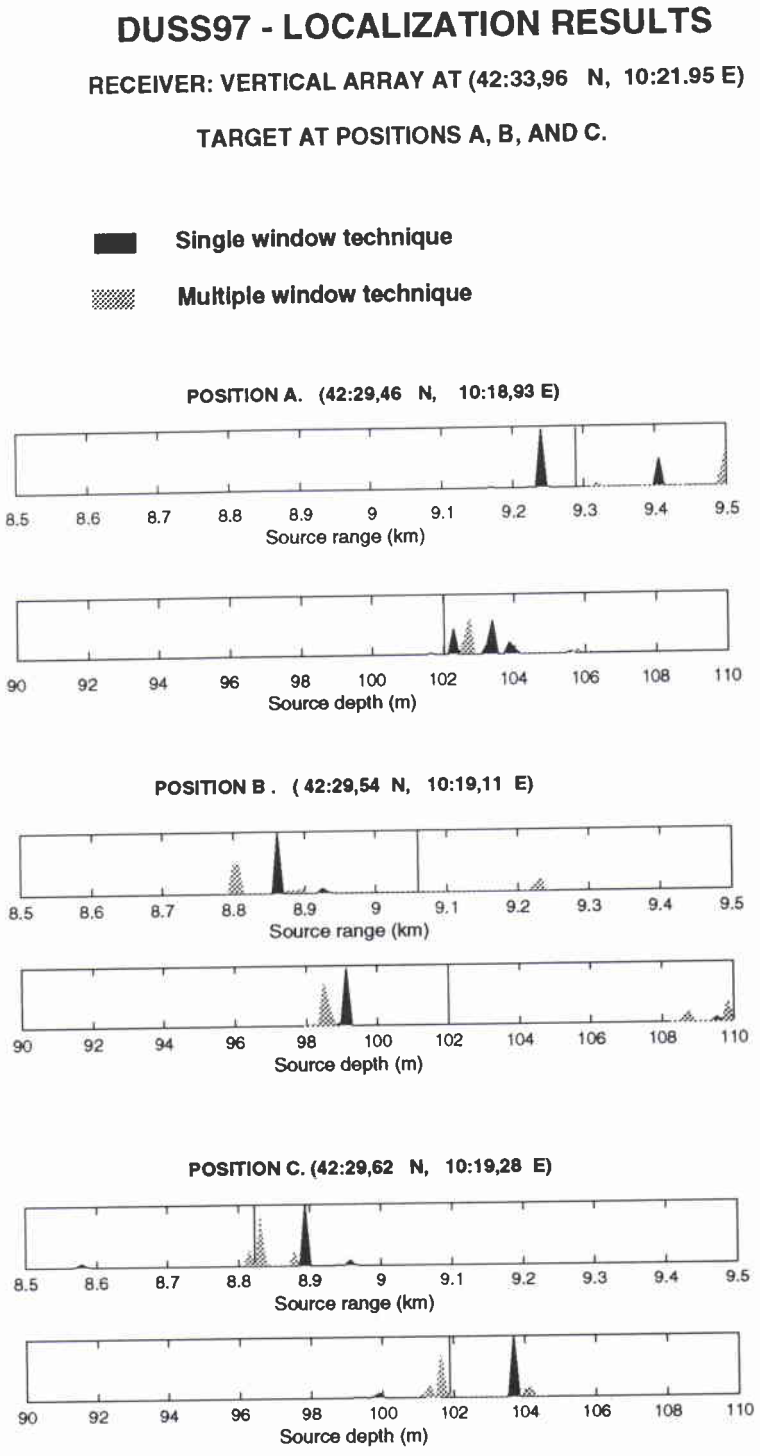

Figure 17 *Comparison of localization results obtained using DPSS tapers with those obtained using the standard technique described in the previous section.*

6 Conclusions

MFP in conjunction with SAGA global search algorithms is used for source localization and environmental inversion, applied to data acquired during a sea trial in July 1997. A slowly moving source is located approximately 9 km from a vertical line receiver array. The estimated positions of the source demonstrate minor deviations from actual values. The environmental inversion is found to be more challenging because of the complex structure of the subbottom layers. However most of the estimated parameter values are close to historical values.

The results demonstrate sensitivity to the number of frequencies processed and to minor changes in the simulation geometry. The most accurate parameter estimation is obtained using the best (highest power) two frequencies. A robust technique for the calculation of the cross-spectral matrix was implemented. The application of this new technique did not improve the stability of the results.

Discrepancies between the calculations of the forward field using C-SNAP and the model incorporated into SAGA, suggest that the parameter variation problem may be related to insufficient accuracy in the calculation of the outgoing acoustic field. Future incorporation of C-SNAP (coupled mode, range dependent model) into the SAGA algorithm could provide more reliable inversion results.

It is shown that in a complex, shallow water environment, the utilization of global inversion methods is an efficient technique to simultaneously solve localization and environmental inversion problems.

References

[1] Tolstoy, A. *Matched Field Processing for Underwater Acoustics* World Scientific Pub, Singapure, 1993.

[2] Tolstoy, A. Review of matched field processing for environmental inverse problems, *International Journal of Modern Physics C*, Vol. 3 (4), pp 691-708, World Scientific Pub, 1992.

[3] Tolstoy, A. Using matched field processing to determine shallow water environmental properties, *2nd International Conference on Theoretical and Computational Acoustics*, 8, World Scientific Pub 1995.

[4] Gerstoft, P. Inversion of seismoacoustic data using genetic algorithms and a posteriori probability distributions *Journal of the Acoustical Society of America* 95(2), pp. 770-782, Feb. 1994

[5] Gerstoft, P. SAGA User manual 2.0 An inversion software package *SACLANTCEN* SM-333, 1997.

[6] Jensen, F. B., and Ferla, C. M. SNAP—The SACLANTCEN normal mode acoustic propagation model, *SACLANTCEN* SM-121 1979.

[7] Ferla, C. M., Porter, M.B., and Jensen, F.B., C-SNAP: Coupled SACLANTCEN normal mode propagation loss model, *SACLANTCEN* SM-274 1993.

[8] Mozzone L., and Bongi, S. Deployable underwater surveillance systems - analysis of experimental results. Parts I and II, *SACLANTCEN* SR–278, SR–283. 1998.

[9] Akal, T., Gehin, C., Matteucci, B., and Tonarelli, B. Measured and computed physical properties of sediment cores, Island of Elba zone, *SACLANTCEN* SM-82, 1972.

[10] Hermand, J.-P., and Gerstoft, P. Inversion of Broad-Band Multitone Acoustic Data from the YELLOW SHARK Summer Experiments *IEEE J. Oc. Eng.* , 21(4), 1996.

[11] Hermand, J.-P., and Soukup, R. Broad-band inversion experiment Yellow Shark '95: Modeling the transfer function of a shallow-water environment with a range-dependent soft clay bottom *Proc. 3rd Europ. Conf. on Underwater Ac.* , J. Papadakis (ed.), Heraklion, Crete, 1996.

[12] Hermand, J.-P., Spina, F., Nardini, P., and Baglioni, E. Yellow Shark broadband inversion experiment: Environmental data 1994-1995 *SACLANTCEN* CD-ROM 1995.

[13] Gingras, D.F. Methods for predicting the sensitivity of matched-field processors to mismatch *Journal of the Acoustical Society of America* 86(5), pp. 1940-1949, Nov. 1989

[14] Gerstoft, P., and Gingras. D.F. Parameter estimation using multifrequency range-dependent acoustic data in shallow water *Journal of the Acoustical Society of America* 99(5), pp. 2839-2850, 1996.

[15] Baggeroer, A.B., Kuperman, W.A., and Schmidt, H. Matched field processing: Source localization in correlated noise as an optimum parameter estimation problem *Journal of the Acoustical Society of America* 83(2), pp. 571-587, 1988.

[16] Böhme, J.F. Statistical array signal processing of measured sonar and seismic data *Proc. SPIE 2563 Advanced Signal Processing Algorithms*, San Diego, 1995.

[17] Davis, L. (ed.) *Handbook of Genetic Algorithms.* Van Nostrand Reinhold, New York, 1991.

[18] Jensen, F.B., Kuperman, W.A., Porter, M.B., Schmidt, H. *Computational Ocean Acoustics*, American Institue of Physics Press, New York, 1994.

[19] Haralabus G., and Gerstoft P. Variability of multi-frequency estimates in shallow water *Proc. of the 3rd European Conference on Underwater acoustics*, Heraklion, Crete, 1996.

[20] Brillinger, D.R. *Time series: Data Analysis and Theory* Holden-Day, San Francisco 1981.

[21] Thomson, D. J. Spectrum Estimation and Harmonic Analysis *Proceedings of the IEEE*, 70(9), pp. 1055-1096, September 1982.

[22] Slepian, D. Prolate Spheroidal Wave Functions, Fourier Analysis and Uncertainty-Part V:The Discrete Case., *Bell System Tech. J.* , 57, pp.1371-1429, 1978.

[23] Percival, D., and Walden, A. *Spectral Analysis for Physical Applications, Multitaper and Conventional Univariate Techniques*, Cambridge University Press, 1993.

[24] Golub, G.H., and Van Loan, C.F. *Matrix Computations* John Hopkins University Press, Baltimore, 1989.

[25] Bell, B., Percival, D.B., and Walden, A.T. Calculating Thomson's Spectral Multitapers by Inverse Iteration *J. Comput. and Graph. Stat.* (Section 1.2), 1993.

[26] Collins, M. D., and Kuperman, W.A. Focalization: Environmental focusing and source localization *Journal of the Acoustical Society of America* 90(3), pp. 1410-1422, 1991.

Report no. changed (Mar 2006): SM-349-UU

Document Data Sheet

NATO UNCLASSIFIED

Security Classification		Project No.
UNCLASSIFIED		041-2
Document Serial No.	**Date of Issue**	**Total Pages**
SM-349	August 1998	36 pp.

Author(s)

Waldhorst, A., Haralabus, G.

Title

DUSS97: Source localization and environmental inversion using vertical array data.

Abstract

Results on source localization and environmental inversion using experimental data acquired on a vertical line array are presented. Global inversion methods based on genetic algorithms are utilized to estimate the range and depth of a moving source located at approximately 9.0 km from the receiver array. Geometric and environmental parameters are estimated. The results are found to be in good agreement with observed values. However, the results are sensitive to minor changes in the simulation geometry and the number of significant frequencies processed. An advanced, non-parametric spectral estimation technique which improved the accuracy of the estimation of the covariance matrix did not enhance localization performance.

Keywords

Localization – global inversion – genetic algorithms – advanced non parametric spectral estimation

Issuing Organization

North Atlantic Treaty Organization
SACLANT Undersea Research Centre
Viale San Bartolomeo 400, 19138 La Spezia, Italy

[From N. America: SACLANTCEN (New York) APO AE 09613]

Tel: +39 0187 527 361
Fax:+39 0187 524 600

E-mail: library@saclantc.nato.int

Initial Distribution for SM 349

Scientific Committee of National Representatives

SCNR Belgium	1	***National Liaison Officers***	
SCNR Canada	1		
SCNR Denmark	1	NLO Canada	1
SCNR Germany	1	NLO Denmark	1
SCNR Greece	1	NLO Germany	1
SCNR Italy	1	NLO Italy	1
SCNR Netherlands	1	NLO Netherlands	1
SCNR Norway	1	NLO Spain	1
SCNR Portugal	1	NLO UK	3
SCNR Spain	1	NLO USA	4
SCNR Turkey	1		
SCNR UK	1	Sub-total	30
SCNR USA	2	SACLANTCEN library	21
French Delegate	1		
SECGEN Rep. SCNR	1		
NAMILCOM Rep. SCNR	1	**Total**	51